Carbohydrate Polymers 111 (2014) 288–297

Contents lists available at ScienceDirect

Carbohydrate Polymers

journal homepage: www.elsevier.com/locate/carbpol

Composite chitosan/silk fibroin nanofibers for modulation of osteogenic differentiation and proliferation of human mesenchymal stem cells

Guo-Jyun Lai [a], K.T. Shalumon [a], Shih-Hsien Chen [a], Jyh-Ping Chen [a,b,*]

[a] Department of Chemical and Materials Engineering, Chang Gung University, Kweishan, Taoyuan 333, Taiwan, ROC
[b] Research Center for Industry of Human Ecology, Chang Gung University of Science and Technology, Kweishan, Taoyuan 333, Taiwan, ROC

ARTICLE INFO

Article history:
Received 25 February 2014
Received in revised form 7 April 2014
Accepted 27 April 2014
Available online 4 May 2014

Keywords:
Chitosan
Silk fibroin
Electrospinning
Human mesenchymal stem cells
Bone tissue engineering
Composite nanofiber

ABSTRACT

Nanofibrous membrane scaffolds of chitosan (CS), silk fibroin (SF) and CS/SF blend were prepared by electrospinning and studied for growth and osteogenic differentiation of human bone marrow mesenchymal stem cells (hMSCs). The morphology and physico-chemical properties of all membrane scaffolds were compared. The influence of CS and SF on cell proliferation was assessed by the MTS assay, whereas osteogenic differentiation was determined from the Alizarin Red staining, alkaline phosphatase activity and expression of osteogenic marker genes. The osteogenic differentiation and proliferation of hMSCs were enhanced by CS and SF nanofibers, respectively. Blending CS with SF retained the osteogenesis nature of CS without negatively influencing the cell proliferative effect of SF. By taking advantage of the differentiation/proliferation cues from individual components, the electrospun CS/SF composite nanofibrous membrane scaffold is suitable for bone tissue engineering.

1. Introduction

Tissue engineering is a scientific domain/field for the repair or regeneration of damaged tissues, which can facilitate the substitution at the damaged sites by engineered tissues with suitable characteristics. These engineered tissues are aimed to restore the functions during the regeneration process, followed by subsequent integration with the host tissue. In bone tissue engineering, scaffolds provide temporary architecture for bone-forming cells to penetrate, adhere and proliferate to form new bone tissues. Hence, the scaffold design should provide a structure suitable for osteogenic differentiation through appropriate cell-materials interactions. The pore size of the scaffold should be adequate for free diffusion of nutrients into and wastes out of the scaffold. The scaffold should also provide requisite mechanical supports and mimic the composition and structure of extracellular matrix (ECM), allowing cells to proliferate, differentiate and maintain their cellular functions. In response to this concern, significant attentions have been given to the development of various polymer scaffolds for biomedical applications (Langer & Vacanti, 1993; Lee & Kim, 2011).

Recent studies show that nanofibrous membrane scaffolds are excellent substrates for bone tissue engineering due to the relevance of nanofiber topography in mimicking the ECM structure (Li, Laurencin, Caterson, Tuan, & Ko, 2002; Zhang, Lim, Ramakrishna, & Huang, 2005). Many biodegradable polymers are currently used for nanofibers development. Among them, natural and synthetic biodegradable polymers were investigated to evaluate the potential of the nanostructured scaffolds in soft (Kumbar, James, Nukavarapu, & Laurencin, 2008) and hard tissue engineering (Lee et al., 2005; Rim, Shin, & Shin, 2013; Cheng et al., 2014). Bone tissue ECM is composed of an organic phase made of type I and type III collagen, glycosaminoglycans (GAGs) and an inorganic calcium phosphate derivative called hydroxyapatite (Porter, Ruckh, & Popat, 2009). A successful impregnation of differentiation and proliferation factors with the nanoscale structures could resolve the difficulties of bone tissue engineering.

Chitosan (CS) is an ideal polymer for biomedical application due to its biocompatibility and biodegradability, along with the osteoconductive and the intrinsic antibacterial nature. It is a linear polysaccharide, composed of glucosamine and *N*-acetyl glucosamine linked in a β(1–4) manner, with the glucosamine/*N*-acetyl glucosamine ratio being referred to as the degree of

* Corresponding author at: Chang Gung University, Chemical and Materials Engineering, 259 Wen Hwa 1st Rd., Kwei-San, Taoyuan, Taiwan. Tel.: +886 3 2118800; fax: +886 3 2118668.
E-mail addresses: jpchen@mail.cgu.edu.tw, jpchen1125@hotmail.com (J.-P. Chen).

http://dx.doi.org/10.1016/j.carbpol.2014.04.094
0144-8617/

deacetylation. The cationic nature of CS is primarily responsible for its electrostatic interactions with anionic GAGs, which is of great interest due to the fact that a large number of cytokines/growth factors are linked to GAGs. A membrane scaffold incorporating CS may therefore retain and concentrate growth factors secreted by the colonizing cells (Madihally & Matthew, 1999). Chitosan was found to promote cell growth and mineral-rich matrix deposition by osteoblasts in culture and showed positive influence on osteogenesis *in vitro* and *in vivo* (Di Martino, Sittinger, & Risbud, 2005). Human osteoblasts grown on CS membranes sustained a spherical morphology and preserved type I collagen expression (Lahiji, Sohrabi, Hungerford, & Frondoza, 2000). Chitosan membranes also promoted the differentiation of osteoprogenitor cells and bone formation (Amaral, Lamghari, Sousa, Sampaio, & Barbosa, 2005).

However, the inferior mechanical properties and high swelling ability that causes easy deformation of CS, present the difficulties to use CS as a membrane scaffold material alone. Polymer blends of CS with other biopolymers such as hyaluronic acid (Yamane et al., 2005), alginate (Li, Ramay, Hauch, Xiao, & Zhang, 2005), gelatin (Huang, Onyeri, Siewe, Moshfeghian, & Madihally, 2005) and silk fibroin (Bhardwaj & Kundu, 2011) have been suggested to develop a more robust composite scaffolds to improve those shortcomings. By combining with other biopolymers, CS can still retain its osteogenesis characteristic but with improved mechanical properties (Chen, Chen, & Lai, 2012). Hence, a blend of CS/biopolymer will be a feasible approach to develop a composite scaffold for bone tissue engineering considering both the biomechanical and tissue regeneration capability of the scaffold.

Silk fibroin (SF) is one of the natural fibrous proteins used as a biomaterial for various biomedical applications (Omenetto & Kaplan, 2010). It is one of the two proteins secreted by silk worm with the other one being sericin. It consists of an amino acid sequence $(Gly–Ser–Gly–Ala–Gly–Ala)_n$. Due to the excellent biocompatibility, biodegradability and mechanical strength, SF has been fabricated into various forms like sponges, gels, films and nanofibers for tissue engineering purposes (Bhardwaj & Kundu, 2011; Bhardwaj & Kundu, 2012; Vepari & Kaplan, 2007; Zhang et al., 2011). Also, due to the high oxygen/water permeability and minimal inflammatory reactions *in vivo*, SF was considered to be one of the best materials for skeletal tissue regeneration (Unger et al., 2007). Nanofibers of SF were used to culture osteoblasts, mesenchymal stem cells and chondrocytes to enhance cell attachment and proliferation (Baek, Park, Ki, Park, & Rah, 2008).

The purpose of this study is to develop a clinically relevant electrospun composite nanofibrous membrane scaffold of CS and SF. We postulate that a combinational approach blending CS and SF could enhance the differentiation/proliferation potential of the nano-structured membrane scaffold; *i.e.* CS enhances differentiation while SF regulates proliferation of stem cells. In a previous study, we have already reported the potential of CS and SF in inducing osteogenic differentiation and cell proliferation of human fetal osteoblastic cells in CS/SF blend (Chen, Chen, & Lai, 2012). As a continuation, a selected 50:50 combination of SF and CS was further evaluated in this study for bone regeneration using human bone marrow stem cells (hMSCs). The critical influence of both materials in morphogenesis was analyzed from the *in vitro* response to identify the clinical relevance of the scaffold.

2. Materials and methods

2.1. Materials

Chitosan (degree of deacetylation = 98%) was purchased from Fluka (Switzerland) and *Bombyx mori* silk fiber was obtained from a local agricultural farm in Miaoli County, Taiwan. $NaHCO_3$, $CaCl_2$ and ethanol were bought from Sigma-Aldrich (USA), Showa (Japan) and Echo (Taiwan), respectively. Trifluoroacetic acid (TFA) and dichloromethane (DCM) were procured, respectively, from Alfa Aesar (UK) and J.T. Baker (USA). Dialysis membrane tubes (CelluSep H1) were purchased from Orange Scientific (USA). All chemicals except *B. mori* silk fiber was used as received.

2.2. Preparation of chitosan (CS), silk fibroin (SF) and CS/SF nanofibers

Silk fibroin was prepared from *B. mori* silk fiber by a stepwise purification method. The silk fiber was treated twice with 0.5% (w/w) $NaHCO_3$ solution, followed by distilled water at 70 °C for 30 min to remove sericin (degumming). A mixed solvent system of $CaCl_2/CH_3CH_2OH/H_2O$ at a molar ratio of 1:2:8 was selected for the dissolution of degummed silk. The process was carried out at 70 °C and continued for 6 h, followed by filtration to obtain a SF solution. A cellulose dialysis tube with a molecular weight cut off of 50,000 was used to remove impurities from the SF solution, with change of water every 12 h up for 5 d. The highly concentrated SF solution was lyophilized overnight to get regenerated SF. Chitosan was selected as the counterpart for blending with SF. To make nanofibrous membrane scaffolds, CS, SF and CS/SF, at concentrations 8, 12.5 and 10%(w/w), respectively, were prepared by dissolving in TFA/DCM mixture (7:3, w/w) (Ohkawa, Cha, Kim, Nishida, & Yamamoto, 2004). Chitosan and SF were prepared in a 1:1 mass ratio to get a total polymer concentration of 10%(w/w) for electrospinning. Polymer solutions were placed in a 5 ml syringe with a 22 gauge needle and delivered by a syringe pump in an automatic electrospinning unit (Jyi Goang Enterprise Ltd., Taiwan). A flow rate of 0.5 ml/h and a working voltage 18 kV was applied to deposit nanofibrous membrane scaffolds on an aluminum foil collector kept 12 cm apart from the needle tip. The prepared CS, SF and CS/SF nanofibers were immersed in a solvent mixture of 7%(v/v) ammonia and 75%(v/v) ethanol for 30 min. Ammonia helps to remove the residual TFA and ethanol helps to reduce the water solubility of SF.

2.3. Characterization of nanofibrous membrane scaffolds

2.3.1. Scanning electron microscopy (SEM) and pore size measurement

Nanofibrous membrane scaffolds were cut into square pieces of 0.5×0.5 cm sizes and placed onto an aluminum stub pasted with a conducting carbon tape. An ion sputter coating machine was used to coat gold over the sample for 60 s at 20 mA. Samples fixed on the holder were inserted into a scanning electron microscope (SEM, Hitachi S-3000N) chamber followed by the evacuation of chamber cavity. The morphology of nanofibers was observed at various locations and recorded. The diameters of the fibers were calculated by measuring at least 100 fibers from 10 images using the ImageJ software. Pore size measurement was carried out with capillary flow porometry (PMI CFP-1100-AI, Porous Materials Inc., USA) using a wetting agent of surface tension 21 dynes/cm.

2.3.2. Fourier transform infrared spectroscopy (FTIR)

The FTIR spectrum of CS/SF nanofibers was recorded and compared with control nanofibers from CS and SF. The electrospun nanofiber membrane was cut into a disc shape of ~1.6 cm diameter and the spectrum was recorded over a wavenumber ranging from 800 to 1800 cm^{-1} with a resolution of 2 cm^{-1} using a Horiba FT-730 spectrometer (Horiba, Japan).

2.3.3. X-ray diffraction spectroscopy (XRD)

XRD measurement was recorded on a Siemens D5005 X-ray diffractometer (Bruker, Germany) with Cu $K\alpha$ radiation

(λ = 1.5418 Å). The sample was scanned in the 2θ range of 5–35° at 2°/min.

2.4. Cell culture and expansion

Human bone marrow mesenchymal stem cells (hMSCs) for cell culture studies were purchased from Cellular Engineering Technologies Inc. (USA) (HMSC.BM-500). Cells (5×10^5) were re-suspended in 10 ml of Dulbecco's Modified Eagle Medium (DMEM) containing 1% antibiotics (penicillin–streptomycin) and 10% fetal bovine serum (FBS) in T75 culture flasks. The temperature was maintained at 37 °C in humidified atmosphere while maintaining CO_2 and air content at 5 and 95%, respectively. The culture medium was changed every 2 d till the cell density reached 80–90% confluence. The supernatant was then removed and cells washed with 10 ml of phosphate buffered saline (PBS) three times to remove residuals from the medium, followed by treatment with 0.05% trypsin–EDTA solution. A cell pellet was collected after centrifugation at 1500 rpm for 5 min, followed by removal of supernatant. A homogenous cell suspension was made by mixing the cell pellet with 1 ml of fresh cell culture medium and re-suspended in three T75 flasks. This cell expansion process was repeated and cells at 3–5 passages were used for all studies.

2.5. In vitro cell culture of hMSCs on nanofibrous membrane scaffolds

2.5.1. Evaluation of cell proliferation by MTS assay

In order to determine the cell proliferation of hMSCs, the number of viable cells was determined using the (3-(4,5-dimethylthiazol-2-yl)-5-(3-carboxymethoxyphenyl)-2-(4-sulfophenyl)-2*H*-tetrazolium) (MTS) assay with the CellTiter 96® Aqueous One Solution Cell Proliferation Kit from Promega (USA). The hMSCs were seeded on 1.6 cm disc-shaped nanofibrous membrane scaffolds placed in 24-well cell culture plates (Nunc) at a seeding density 5×10^3 cells/cm^2 of scaffold and cultured in DMEM, FBS (10%), antibiotic/antimycotic (1%), 0.1 μM dexamethasone, 50 μM L-ascorbic acid phosphate and 10 mM glycerol 2-phosphate osteogenic medium. A sample was taken out and rinsed three times at pre-determined time points (0, 3, 7, 14, 21 and 28 d). A mixture of 200 μl medium and 40 μl MTS reagent was added to each sample and incubated for 3 h at 37 °C. The MTS reagent was reduced by live cells into a colored formazan product and the optical density (OD) was measured at 492 nm using an ELISA reader (Synergy HT, BioTek, USA).

2.5.2. Laser scanning confocal microscopy

Qualitative measurement of cell viability was determined using the LIVE/DEAD® Viability/Cytotoxicity Kit for mammalian cells (Molecular Probes, USA). Cells were cultured in membrane scaffolds for three days, followed by removal of the medium and PBS washing for three times. The assay reagent was prepared by mixing 5 μl of ethidium homodimer (EthD-1) and 3 μl calcein AM in 10 ml culture medium, followed by addition of 1 ml of reagent to each well in 24-well plates for staining live (green) and dead (red) cells. The whole process was performed in dark and the membrane scaffolds incubated with the reagent at 37 °C for 30 min. After the incubation period, cell-membrane scaffolds were observed under a confocal laser scanning microscope (Zeiss LSM 510, Germany). The excitation/emission wavelength were 528/617 nm for EthD-1 and 494/517 nm for calcein AM.

For cytoskeleton staining, cell-membrane scaffolds were treated with 4% paraformaldehyde in PBS for 20 min, followed by dehydration with ethanol and permeabilization with 0.1% Triton X-100 for 5 min. Cytoskeleton was stained with 50 μg/ml phalloidin–tetramethylrhodamine B isothiocyanate (TRITC) (Sigma-Aldrich) solution for 30 min at room temperature and then washed with PBS to remove unreacted phalloidin conjugates. Nuclear staining was done with DAPI with the VECTASHIELD® mounting medium. Fluorescent images were recorded at excitation/emission wavelength of 540/570 nm for phalloidin and 360/460 nm for DAPI.

2.5.3. Alkaline phosphatase (ALP) activity

The intracellular ALP activity was measured using an ALP assay kit (SensoLyte®) from AnaSpec (USA). Membrane scaffolds were seeded with hMSCs at a density of 5×10^3cells/cm^2 in 24-well plates and cultured in the osteogenic medium. Samples were taken for analysis at 0, 3, 7, 14, 21 and 28 d and washed with PBS. Membrane scaffolds with cells were immersed in 500 μl cell lysis solution containing 0.1% Triton X-100 and 5 mM $MgCl_2$. The whole solution was transferred to a tube and centrifuged at 13,000 rpm for 10 min at 4 °C. ALP activity was measured by mixing 50 μl of supernatant with 50 μl *p*-nitrophenyl phosphate (5 mM) in 150 mM 2-amino-2-methyl-1-propanol buffer solution at room temperature for 30 min in dark. Following the incubation period, the reaction was stopped by adding 50 μl of 0.2 N NaOH to denature ALP and the OD was measured at 405 nm using an ELISA reader. By normalizing to the cell number from the MTS assay, specific ALP activity per cell basis was reported and expressed as OD_{405}/OD_{492}.

2.5.4. Mineralization of hMSCs

All membrane scaffolds were cultured with hMSCs at 5×10^3 cells/cm^2 density in 24-well plates in osteogenic medium to evaluate cell mineralization at three time points (7, 14 and 21 d). At every specific time point, membrane scaffolds were rinsed with PBS and fixed with 4% glutaraldehyde at room temperature for 2 h. Samples were washed with PBS for three times for 20 min and post-fixed in 1% osmium tetroxide (in 0.1 M phosphate buffer) at room temperature for 2 h, followed by washing with distilled water for three times (20 min each). Alcohol gradient drying was performed to remove water from membrane scaffolds at increasing ethanol concentrations (50, 70, 80, 90, 95 and 100%). A critical point dryer was used for final drying, to make the sample ready for sputter coating. The sample was coated with gold at 20 mA for 60 s, followed by examination in SEM (Hitachi S-3000N, Japan). Atomic percentages of elements in mineral deposits on nanofiber surface were determined from energy dispersive X-ray analysis (EDX) (Horiba EX-250, Japan).

Cell-membrane scaffolds were subject to Alizarin Red staining for calcium content at 14, 21 and 28 d of culture after binding mineralized calcium salts in membrane scaffolds with Alizarin Red S (ARS). Membrane scaffolds were washed three times with PBS and fixed with 2.5% glutaraldehyde solution (dissolved in 0.1 M phosphate buffer) for 2 h. 0.5 g of ARS was dissolved in 25 ml deionized water and the pH was adjusted to 4.1–4.3 with 10% ammonium hydroxide. One milliliter of ARS solution was added to each well, followed by incubation for 1 h at room temperature. Deionized water was used to wash off the excess dye adsorbed on the membrane scaffold surface. Presence of mineral deposition was qualitatively evaluated using the intensity of red color on the surface after taking photomicrographs using an inverted microscope (Olympus IX-71, Japan). Calcium quantification was measured using cetylpyridinium chloride (CPC) treatment. ARS-stained membrane scaffolds were washed with deionized water and followed by treatment with 1 ml of 10% CPC solution for 1 h to desorb calcium ions. Absorbance of the solution was read at 540 nm in an ELISA reader (OD540) and normalized to the cell number from the MTS assay (OD_{540}/OD_{492}).

Table 1
Primer sequences of Col I, ALP, OCN, OPN and GAPDH used for Q-PCR.

Gene	Gene ID	Forward/reverse
Collagen type I (COL I)	NM_000089	GTGGTGACCAAGGTCCAGTT/CACCTGGTAGACCACGTTCA
Alkaline phosphatase (ALP)	NM_000478	TGCAGTACGAGCTGAACAGG/GTCAATTCTGCCTCCTTCCA
Osteocalcin (OCN)	NM_199173	GGCAGCGAGGTAGTGAAGA/TCAGCCAACTCGTCACAGTC
Osteopontin (OPN)	NM_001040060	TCAGCTGGATGACCAGAGTG/TTGGGGTCTACAACCAGCAT
Glyceraldehyde 3-phosphate dehydrogenase (GAPDH)	NM_002046	TGTTCGTCATGGGTGTGAAC/GTCTTCTGGGTGGCAGTGAT

2.5.5. Gene expression by quantitative PCR (Q-PCR)

Expression of osteogenic marker gene was quantified by Q-PCR after RNA isolation and cDNA synthesis as per standard procedures. Briefly, RNA was isolated from samples after cultured for 2 and 3 weeks in 24-well plates using TRIzol (Invitrogen, USA). Cell suspension was transferred to a 1.5 ml microcentrifuge tube, followed by the addition of 200 μl chloroform and vortexing for 15–30 s to disrupt cell membrane. The tube was placed in an ice bath for 5 min and centrifuged at 11,000 rpm for 15 min. Among the three layers, the supernatant containing RNA was isolated and reacted with isopropanol in 1:1 ratio for 30 min at −80 °C, followed by centrifugation at 11,000 rpm for 15 min at 4 °C. The supernatant was removed and 1 ml 75% ice cold ethanol (diluted with diethyl pyrocarbonate treated water) was added and mixed for 10 min at 4 °C, followed by centrifugation at 11,000 rpm for 10 min. The process was repeated twice. The supernatant was removed and the pellet dried at room temperature. Completely dissolved RNA solution was obtained by treating the pellet with 30 μl DEPC treated water (Invitrogen, USA) at 55 °C for 15 min. One microgram of total RNA was reverse-transcripted into cDNA using SuperScript III RNase H (Invitrogen, USA). Primers used were for collagen type I (Col I), ALP, osteocalcin (OCN) and osteopontin (OPN). Q-PCR was performed using a SYBR®Green RT-PCR kit (SYBR Green I supermix, Bio-Rad) and a MiniOption detection system (Bio-Rad CFD-3120). Comparative threshold cycle method was used to analyze the results using Bio-Rad software with GAPDH as the housekeeping gene. All results were quantified using the $2^{-\Delta\Delta ct}$ relative quantification method. The primer sequences are shown in Table 1.

2.6. Statistical analysis

All quantitative data were expressed as mean ± standard deviation. Statistical analysis was performed using the one-way ANOVA LSD test to determine significant differences. A value of $p < 0.05$ was considered statistically significant.

3. Results and discussion

3.1. Preparation and characterization of CS, SF and CS/SF nanofibers

Nanofibers of CS, SF and CS/SF were prepared at the optimum electrospinning condition and fiber morphology was observed under SEM. The surface morphology of nanofibers was smooth and beads-free in nature. Chitosan nanofibers were prepared from 8% solution whereas SF nanofibers from 12.5%. An optimized polymer concentration (10%) was selected to obtain CS/SF nanofibers at 1:1 mass ration. The diameter observed for each fiber type was 316.67 ± 109.19 nm for CS, 398.60 ± 183.80 nm for SF, and 446.93 ± 167.48 nm for CS/SF nanofibers with no significant difference in fiber diameter among the membrane scaffolds (Fig. 1A). The pore sizes measured by capillary flow porometry were 0.52 ± 0.10, 0.98 ± 0.21 and 0.71 ± 0.18 μm for CS, SF and CS/SF membrane scaffolds, respectively. A mixed solvent system of ammonia/ethanol was used for post-treatment to remove residual TFA from the nanofiber to avoid cellular toxicity and to insolubilize SF in water by converting the α-helical protein structure to the β-sheet form

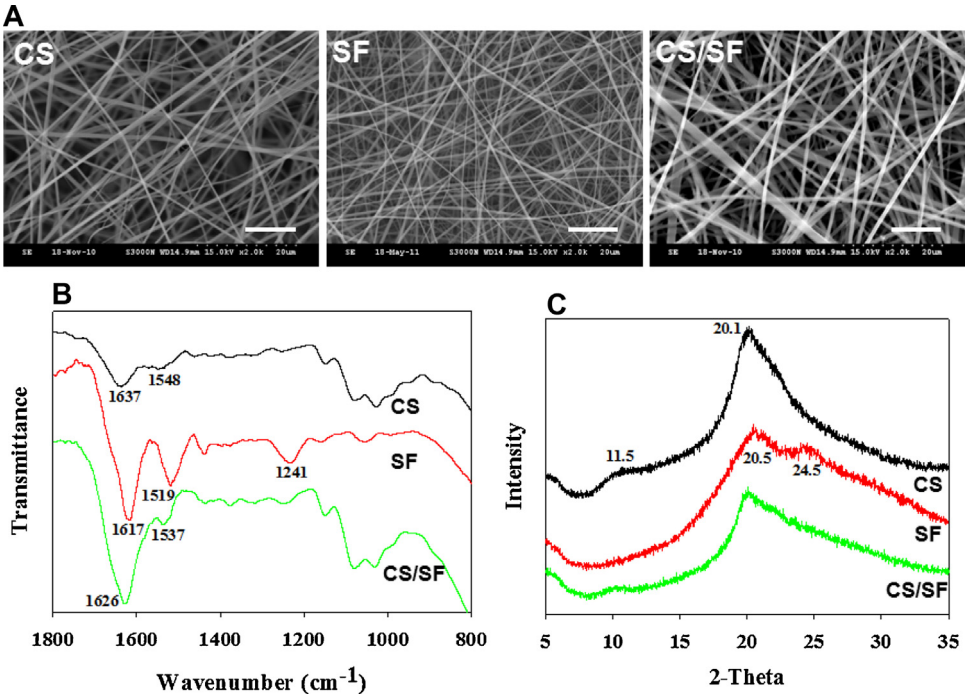

Fig. 1. (A) SEM photomicrographs, (B) FTIR spectra and (C) XRD diffraction peaks of electrospun nanofibrous membrane scaffolds of chitosan (CS), silk fibroin (SF) and CS/SF. Bar = 10 μm.

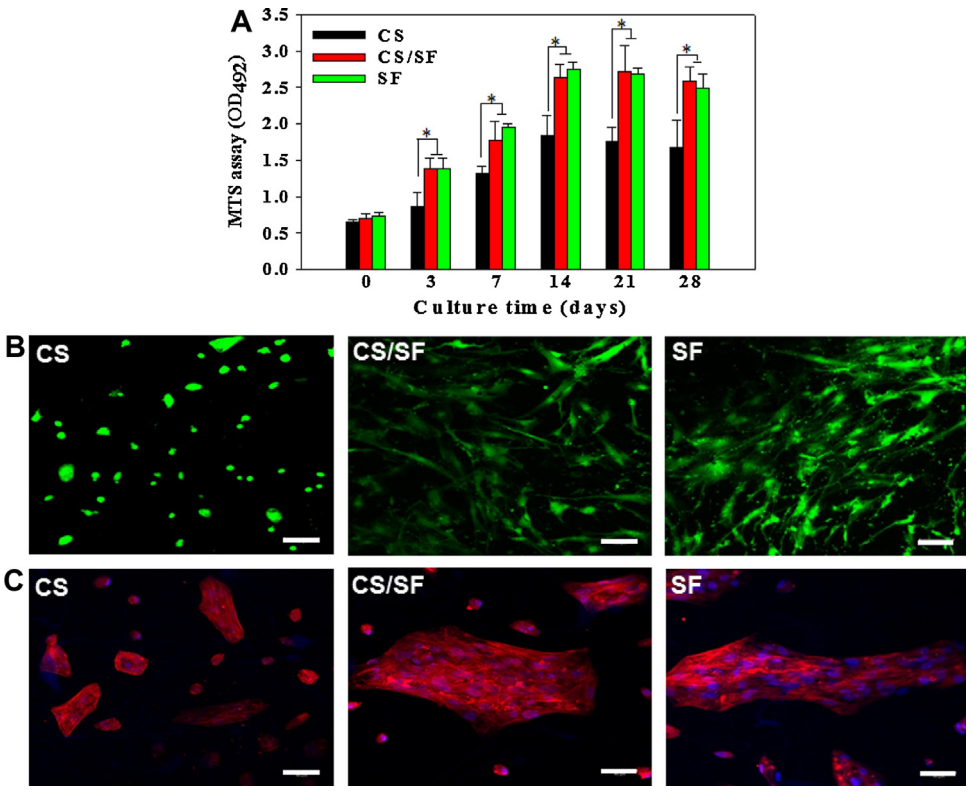

Fig. 2. (A) Proliferation of hMSCs in electrospun chitosan (CS), silk fibroin (SF) and CS/SF nanofibrous membrane scaffolds by MTS. CS membrane scaffold has significant fewer cells compared to CS/SF and SF membrane scaffolds. (B) Live-dead and (C) phalloidin-DAPI staining of hMSCs cultured in electrospun CS, SF and CS/SF nanofibers membrane scaffolds at day 3. A high cell proliferation potential was observed for SF and CS/SF and the cell morphology is spindle-shaped with well-organized fibrous F-actin cytoskeleton. Bar is 100 μm in (B) and 50 μm in (C). * $p < 0.05$.

(Hasegawa, Isogai, Onabe, & Usuda, 1992; Matsuda, Kagata, Kino, & Tanaka, 2007). De-protonation of amino groups in alkaline solutions could lead to imply the complete removal of TFA. The thickness of the prepared membranes was in the range of 150 to 200 μm.

The characteristic functional groups present in each membrane scaffold were monitored by FTIR. Complete removal of TFA from nanofibers after ammonia treatment was confirmed from the absence of transmittance peaks associated with TFA salts (720, 796, and 836 cm^{-1}) (Chen, Chen, & Lai, 2012) (Fig. 1B). The characteristic transmittance peaks of CS are stretching of C=O and NH_2 at around 1637 and 1548 cm^{-1} (Jeong, Lee, Liu, & Park, 2006; She et al., 2008). Similarly, the transmittance peaks of SF can be observed at 1617 (amide I), 1519 cm^{-1} (amide II) and 1241 cm^{-1} (amide III). The presence of transmittance peaks at 1617 and 1519 cm^{-1} after ethanol treatment indicates β-sheet protein conformation in SF rather than random coils that would show transmittance peaks at 1650 (amide I) and 1535 cm^{-1} (amide II) (Jeong et al., 2006). The transmittance peaks of CS/SF show characteristic peaks from both CS and SF. The SF peaks shift to 1626 and 1537 cm^{-1}, confirming again the conformation change of SF in the composite nanofibers after chemical treatment, and the C=O and NH_2 stretching bands of CS merge with SF bands in the composite (Chen, Chen, & Lai, 2012).

The CS, SF and CS/SF nanofibrous membranes were analyzed by XRD, which reveals four distinct peaks in the region from 5 to 35° (Fig. 1C). The structure of CS was identified by the presence of peaks at 11.5 and 20.1° while the diffraction peaks at 20.5° and 24.5° point toward the presence of SF (Kundu, Chung, Kim, Tae, & Kundu, 2010). The CS/SF composite shows diffraction peaks from both CS and SF with domination of CS over SF in determining the structure of the composite nanofibers. The result also indicates a well dispersed behavior of CS and SF in the CS/SF nanofibrous membrane.

3.2. In vitro cell culture

3.2.1. Cell proliferation

Cytotoxicity of nanofibers toward hMSCs from the MTS assay is shown in Fig. 2A. The number of viable cells at day 0 (after 4 h cell attachment) was taken as a reference point to compare the proliferation rate of hMSCs on various nanofibers. The cell number increased with culture time (Bhattarai, Edmondson, Veiseh, Matsen, & Zhang, 2005) but exhibits a material dependence or an effect of nanofiber composition on cell proliferation rate. At day 0, the viable cell number was not significant different among nanofibers, indicating cell attachment to nanofibrous membrane scaffolds is similar. Upon cell growth, from day 3, a significant difference ($p < 0.05$) in cell number was observed between CS and SF nanofibers as well as between CS and CS/SF nanofibers. Nonetheless, no significant difference between SF and CS/SF nanofibers was found. The maximum cell number was attained at 14 d where cells exhibited growth arrest thereafter. The results demonstrate enhanced cell proliferation capability of SF toward hMSCs compared with CS. The elevated cell number for both SF and CS/SF membrane scaffolds indicates that although CS is not beneficial for cell proliferation, it does not hamper the enhanced cell conductivity of SF in composite CS/SF nanofibers.

3.2.2. Cellular viability and morphology

Assessments of cellular viability and morphology were performed to evaluate electrospun nanofibers as cellular membrane scaffolds. Although there is no difference in cell viability among different membrane scaffolds from live–dead staining results (Fig. 2B), more spindle-shaped cells were found in the CS/SF and SF nanofibers than in CS nanofibers where cells changed to a cuboidal shape. The difference in cell number is consistent with the

difference in the cell proliferation rate observed in Fig. 2A. The morphology difference of attached cells was further confirmed when cells were stained with DAPI and phalloidin for nuclear and F-actin staining, respectively (Fig. 2C). Cells in the CS membrane scaffold show a diffused F-actin cytoskeletal organization; in contrast, cells in SF and CS/SF membrane scaffolds demonstrate enhanced cellular spreading and a well-organized fibrous F-actin cytoskeleton. Cell spreading on materials affects cell functions, including proliferation and differentiation. Also, cell spreading is related to filopodia extension which has been shown to be dependent on substrate properties. Therefore, SF-containing nanofibers facilitate an adequate environment for cell growth and production of ECM (Bhardwaj & Kundu, 2011). In contrast, the cell phenotype in CS membrane scaffold is comparatively rounded with differentiation presiding over proliferation. In other words, CS contributes to cell differentiation while SF promotes cell proliferation. A composite CS/SF membrane scaffold will be the ideal scaffold that helps cellular attachment, growth and differentiation toward the osteogenic lineage, wherein being alone, CS and SF are not effective. Similar results explaining the effect of CS on cell proliferation was reported by Zhang et al. (2010). A separate study reported the effect of CS concentrations on the relative cell viability of AH927 on SF/CS scaffolds. It suggested that increase in concentration of CS decreased the cell viability, or increase in SF composition favored cell proliferation (Bhardwaj & Kundu, 2011). Our results suggest the individual contribution of CS and SF in CS/SF composite nanofibers for differentiation and proliferation of hMSCs.

3.2.3. Alkaline phosphatase (ALP) activity

ALP plays a crucial role in the initiation of the mineralization process by cell differentiation. Calcification occurs at the site of nucleation as a result of accumulation of inorganic phosphates and Ca^{2+} (Malaval, Liu, Roche, & Aubin, 1999; Ogata et al., 2005). The mechanism is through the hydrolysis of phosphate esters by ALP to increase the phosphate concentration in local environment and thus elevating the mineralization of ECM (Ogata et al., 2005). ALP enzyme is a transcription factor that activates the downstream cell differentiation factor and it also takes part in message delivery, followed by promoting the differentiation of osteoblasts. Due to this, ALP can be considered as an early interim osteoblast activity indicator. The ALP activity of hMSCs cultured in CS, CS/SF and SF nanofibrous membrane scaffolds was shown in Fig. 3A and B. For total ALP activity measurement, during culture period from day 3 to 28, there was no significant difference in OD values between CS and CS/SF, but a significant difference was found between those groups and the SF group (Fig. 3A). This suggests the effect of CS on the differentiation of hMSCs (Bhardwaj & Kundu, 2011). The normalized ALP values corresponding to cell number is given in Fig. 3B. While normalization, in contrast to total ALP values, a significant difference was observed for CS group with SF and CS/SF groups only at day 3. As culture time increased to 7 through 28 days, the ALP activity was significantly different between CS and CS/SF groups and CS/SF and SF groups. The ALP activity per cell basis was thus directly proportional to CS concentration in the membrane scaffold. As the CS concentration was reduced to 50%, the ALP activity also decreased and finally showed the minimum for 0% CS (SF only). In a previous study, the effect of CS concentration on enhanced production of ALP was also reported in hydroxyapatite/collagen/chitosan composites (Zhang et al., 2010).

3.2.4. Mineralization of hMSCs

Mineralization is the process in which calcium phosphate deposits on the surface of substrates (Heinemann et al., 2009; Toskas et al., 2013). One of the evidences of differentiation of hMSC to the osteogenic lineage is their capability to mineralize inorganic phosphates at the middle of the differentiation period. This could be monitored as inorganic mineral deposition in the ECM secreted by cells. The deposition was observed through SEM as an evidence for hMSCs osteogenic differentiation. From Fig. 3C, hMSCs seeded on CS, CS/SF and SF nanofibrous membrane scaffolds show both material and time depended mineralization. The mineralization was found to be the minimum at day 7 and increased with time till day 21. But irrespective of time, the extent of mineralization was specific to the materials present in the membrane scaffold, with abundant mineral deposition only for CS and CS/SF as CS accelerates hMSCs differentiation and mineral deposition even at earlier time points. From SEM images, it is also evident that hMSCs formed filopodia-like extensions to attach to the SF nanofibers, assisting them in spreading and proliferation in the SF nanofibrous membrane scaffold (Chen, Chen, & Lai, 2012; Cheon et al., 2010).

Table 2
Atomic percentages of elements in minerals deposited by hMSCs in CS, CS/SF and SF nanofibrous membrane scaffolds at different culture times.

Culture Time (d)	Element	Membrane scaffold		
		CS	CS/SF	SF
7	C	61.76	60.28	70.92
	O	36.68	37.71	28.79
	P	1.40	1.75	0.20
	Ca	0.16	0.26	0.09
14	C	42.02	58.00	62.13
	O	46.09	32.99	37.05
	P	4.66	5.02	0.67
	Ca	6.23	4.09	0.15
21	C	45.81	45.23	61.05
	O	41.47	43.17	36.45
	P	6.32	6.07	1.82
	Ca	6.40	5.53	0.68

Differentiation of hMSCs to osteoblasts was also evaluated by measuring the atomic percentages of elements in the mineral deposit using EDX analysis (Chen & Chang, 2011). The bone mineral contains calcium phosphate in the form of hydroxyapatite (HAP), which is the major component of cortical bone. The crucial elements present in HAP (Ca and P) could be identified through elemental composition analysis. Fig. 3D is the EDX spectra of mineral deposition of hMSCs cultured in CS, CS/SF and SF nanofibrous membrane scaffolds at 7, 14 and 21 d. The lowest Ca and P peak intensity for SF nanofibers could be observed qualitatively. Table 2 shows the calculated elemental composition in the mineralized ECM for each membrane scaffold. Time dependent mineralization could be confirmed from the increase of P and Ca composition, with elevated values at 14 and 21 d for CS-containing membrane scaffolds. The relatively higher percentage of Ca and P observed for CS and CS/SF further underlines the positive influence of CS on hMSCs differentiation and mineralization.

Mineralization occurs by cell-mediated deposition of ECM components. When hMSCs differentiates on nanofibers, anionic matrix molecules will take up Ca^{2+}, followed by phosphate ions and thus leads to calcification through nucleation and growth (Boskey, 1998). ARS can bind to Ca^{2+} in mineralized ECM, showing bright red stains. Fig. 4 is the optical microscopic images of ARS-stained CS, CS/SF and SF membrane scaffolds, confirming the variations in stain intensity for different membrane scaffolds with respect to time. At day 7, the Alizarin Red stain shows slight reddish dots on both CS and CS/SF membrane scaffolds but almost no positive stains were found over SF. Slightly enhanced staining was observed at day 14 for CS and CS/SF but SF remains the same as before. In contrast, at day 21, both CS and CS/SF membrane scaffolds show intense red staining, providing the material dependent mineralization of hMSCs.

Quantitative cell mineralization was done after extracting ARS with 10% CPC to evaluate calcium-rich mineral deposits by hMSCs

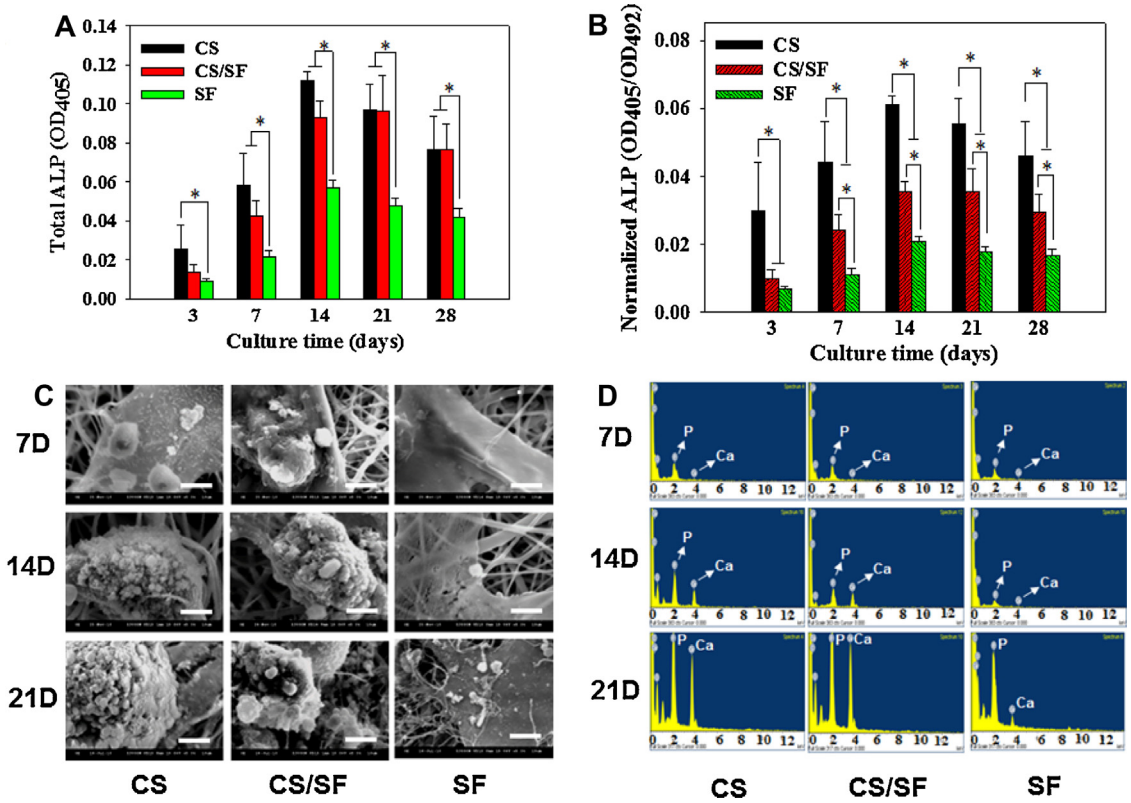

Fig. 3. (A) Total and (B) normalized alkaline phosphatase (ALP) activity of hMSCs cultured on electrospun chitosan (CS), silk fibroin (SF) and CS/SF nanofibrous membrane scaffolds. (C) SEM and (D) EDX analysis of cell mineralization on electrospun CS, SF and CS/SF nanofibrous membrane scaffolds. Bar = 5 μm. * $p < 0.05$.

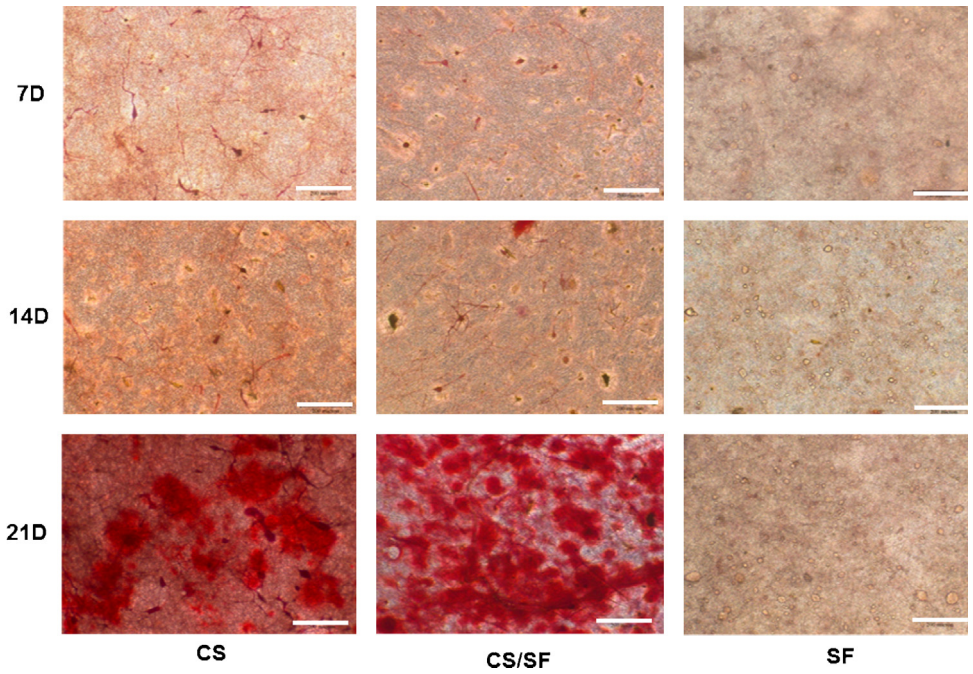

Fig. 4. Alizarin Red staining of hMSCs cultured on electrospun chitosan (CS), silk fibroin (SF) and CS/SF nanofibrous membrane scaffolds at 7, 14 and 21 days indicates CS and CS/SF membrane scaffolds show bright red spots at 7 and 14 days and intense red staining at 21 days. Relatively no positive red staining is found in SF membrane scaffolds. Bar = 200 μm.

(Fig. 5). Calcium quantification was recorded as total calcium content *vs* culture periods, followed by normalized quantitative data with respect to cell number. The total calcium content was found to be increasing with time. At day 14 through 28, the total calcium content in deposited minerals on CS and CS/SF nanofibers were significantly higher than that of SF. At the same time, there was no significant difference in calcium content between CS and CS/SF at all times (Fig. 5A). When normalized to cell number, the mineralization was still found to increase with time but the results were different from total calcium quantification values (Fig. 5B).

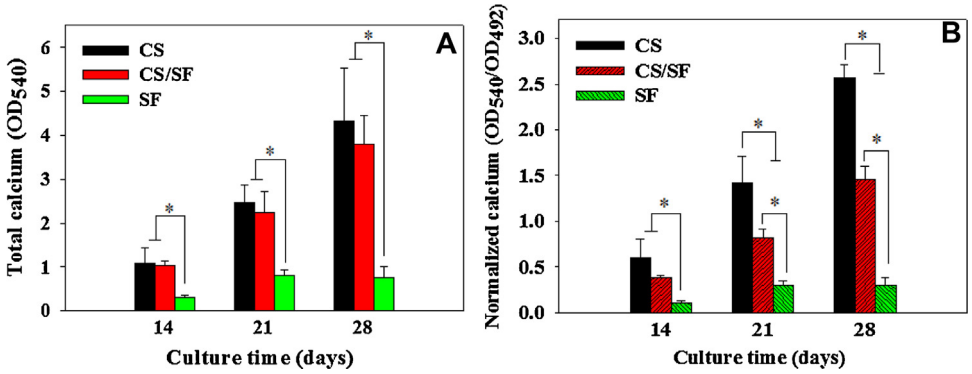

Fig. 5. Quantitative evaluation of mineral deposition from total (A) and normalized (B) calcium content of hMSCs cultured on electrospun chitosan (CS), silk fibroin (SF) and CS/SF nanofibrous membrane scaffolds. CS shows the maximum calcium deposition and SF the minimum at all times, whereas CS/SF has a mid-level calcium deposition. * $p < 0.05$.

At day 14, the trend was the same as total calcium quantification, whereas at day 21 and 28, the deposition was significantly different among three membrane scaffolds with hMSCs exhibit the maximum rate of calcium deposition on CS nanofibers and the minimum on SF as expected. The quantitative assessment of mineral deposition depicts the same trends observed from total and normalized ALP activity (Fig. 3A and B), pointing out the importance of CS in the mineralization process of hMSCs.

3.2.5. Gene expression studies by Q-PCR

The three main characteristics of cellular growth during transformation from stem cells to osteoblasts are cell proliferation, ECM maturation and ECM mineralization. It is accompanied by certain up-regulation or down-regulation of genes in each stage (Setzer, Bächle, Metzger, & Kohal, 2009). Fig. 6 shows the relative gene expression levels of various early, middle and later osteogenic marker genes. The selected mRNA expressions corresponds to specific genes were collagen type I (Col I), ALP, osteopontin (OPN) and osteocalcin (OCN). Col I is an early differentiation marker observed at the initial stage of differentiation whereas ALP is expressed at early and middle stages. OPN expression is observed at the middle/late stage while OCN is at the late stage of differentiation. Cell proliferation helps to produce more ECM and hence it could be compared from measurement of Col I gene expression. In Fig. 6A, at 14 and 21 d, CS shows significantly lower levels of Col I expression compared to CS/SF and SF. This is due to the positive effect of SF on cell proliferation than differentiation as discussed before, *i.e.* SF leads to faster cell growth than CS and more ECM could be produced, therefore, up-regulation of Col I gene is found in SF and CS/SF scaffolds. This is verifiable from the MTS assay in Fig. 2A. Col I gene expression was almost the same at both time points with no significant difference between day 14 and 21 due to its early expression. The expression of ALP was higher in CS and CS/SF, which shows significant difference from that in SF as hMSCs commits toward the osteogenic lineage by the action of CS (Fig. 6B). The ALP level was lower at 21 d compared to 14 d, confirming the early/middle gene

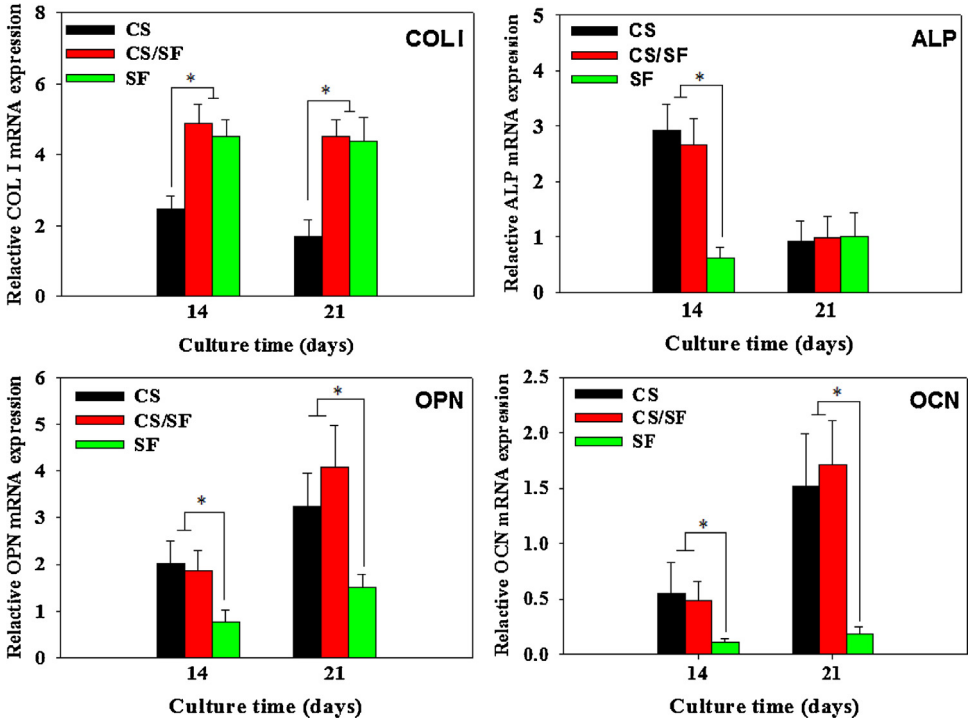

Fig. 6. Type I collagen (Col I), alkaline phosphatase (ALP), osteopontin (OPN) and osteocalcin (OCN) mRNA expression of hMSCs in electrospun chitosan (CS), silk fibroin (SF) and CS/SF nanofibrous membrane scaffolds. The relative Q-PCR values were corrected using the glyceraldehyde-3-phosphate dehydrogenase (GAPDH) expression levels. The values are the mean values ± SD of three independent experiments. * $p < 0.05$.

expression of the same. The levels of OPN and OCN gene expression increased from 14 d to 21 d, confirming the middle/late and late differentiation characteristics of OPN and OCN genes, respectively, during bone formation (Fig. 6C and D) (Karageorgiou et al., 2004; Li, Vepari, Jin, Kim, & Kaplan, 2006). hMSCs cultured on CS-containing nanofibers (CS and CS/SF) showed significant higher levels of gene expression than on SF nanofibers at all times. This behavior reiterates the fact that CS provide a cue for hMSCs differentiation toward osteoblasts, and such mechanism is preserved irrespective of single component CS nanofibers or composite CS/SF nanofibers after blending CS with SF. From the literature, the monomer of chitosan, glucosamine, was also reported to associate with an increase in the expression of osteogenic marker genes during osteogenic differentiation of hMSCs (Lieder et al., 2012).

4. Conclusions

Electrospun CS, SF and CS/SF nanofibrous membrane scaffolds could be fabricated by the electrospinning technique. The physicochemical properties of all membrane scaffolds could be compared from SEM, FTIR, XRD and pore size measurements. Cell culture analysis from cytoskeleton staining and the MTS assay suggest the proliferation cue of SF on hMSCs in the CS/SF nanofibers. From the regulation of ALP activity, mineral deposition and osteogenic gene expression, CS was found to guide hMSCs toward the osteogenic lineage and induce the formation of bone tissue *in vitro*. The results suggest that CS and SF are excellent candidates for proliferation and osteogenic differentiation of hMSCs, respectively. A blend of CS with SF in the composite nanofibers preserved the osteogenesis nature of CS without diminishing the cell proliferative effect of SF. A facile combination of CS and SF in the electrospun nanofibers could therefore result in a promising membrane scaffold for bone tissue development, with CS inducing differentiation and SF promoting proliferation.

Acknowledgments

We are thankful for the financial supports from National Science Council, Taiwan, ROC (NSC-100-2221-E-182-024 and NSC-101-2221-E-182-029) and Chang Gung Memorial Hospital (CMRPD1B0241 and CMRPD1B0242).

References

Amaral, I. F., Lamghari, M., Sousa, S. R., Sampaio, P., & Barbosa, M. A. (2005). Rat bone marrow stromal cell osteogenic differentiation and fibronectin adsorption on chitosan membranes: The effect of the degree of acetylation. *Journal of Biomedical Materials Research A*, *75*, 387–397.

Baek, H. S., Park, Y. H., Ki, C. S., Park, J. C., & Rah, D. K. (2008). Enhanced chondrogenic responses of articular chondrocytes onto porous silk fibroin scaffolds treated with microwave-induced argon plasma. *Surface and Coatings Technology*, *202*, 5794–5797.

Bhardwaj, N., & Kundu, S. C. (2011). Silk fibroin protein and chitosan polyelectrolyte complex porous scaffolds for tissue engineering applications. *Carbohydrate Polymers*, *85*, 325–333.

Bhardwaj, N., & Kundu, S. C. (2012). Chondrogenic differentiation of rat MSCs on porous scaffolds of silk fibroin/chitosan blends. *Biomaterials*, *33*, 2848–2857.

Bhattarai, N., Edmondson, D., Veiseh, O., Matsen, F. A., & Zhang, M. (2005). Electrospun chitosan-based nanofibers and their cellular compatibility. *Biomaterials*, *26*, 6176–6184.

Boskey, A. L. (1998). Biomineralization: Conflicts, challenges, and opportunities. *Journal of Cellular Biochemistry Supplement*, *30–31*, 83–91.

Chen, J. P., & Chang, Y. S. (2011). Preparation and characterization of composite nanofibers of polycaprolactone and nanohydroxyapatite for osteogenic differentiation of mesenchymal stem cells. *Colloids and Surfaces B: Biointerfaces*, *86*, 169–175.

Chen, J. P., Chen, S. H., & Lai, G. J. (2012). Preparation and characterization of biomimetic silk fibroin/chitosan composite nanofibers by electrospinning for osteoblasts culture. *Nanoscale Research Letters*, *7*, 170.

Cheng, Y., Ramos, D., Lee, P., Liang, D., Yu, X., & Kumbar, S. G. (2014). Collagen functionalized bioactive nanofiber matrices for osteogenic differentiation of mesenchymal stem cells: Bone tissue engineering. *Journal of Biomedical Nanotechnology*, *10*, 287–298.

Cheon, Y. W., Lee, W. J., Baek, H. S., Lee, Y. D., Park, J. C., Park, Y. H., Ki, C. S., Chung, K. H., & Rah, D. K. (2010). Enhanced chondrogenic responses of human articular chondrocytes onto silk fibroin/wool keratose scaffolds treated with microwave-induced argon plasma. *Artificial Organs*, *34*, 384–392.

Di Martino, A., Sittinger, M., & Risbud, M. V. (2005). Chitosan: A versatile biopolymer for orthopaedic tissue-engineering. *Biomaterials*, *26*, 5983–5990.

Hasegawa, M., Isogai, A., Onabe, F., & Usuda, M. (1992). Dissolving states of cellulose and chitosan in trifluoroacetic acid. *Journal of Applied Polymer Science*, *45*, 1857–1863.

Heinemann, S., Heinemann, C., Bernhardt, R., Reinstorf, A., Nies, B., Meyer, M., Worch, H., & Hanke, T. (2009). Bioactive silica–collagen composite xerogels modified by calcium phosphate phases with adjustable mechanical properties for bone replacement. *Acta Biomaterialia*, *5*, 1979–1990.

Huang, Y., Onyeri, S., Siewe, M., Moshfeghian, A., & Madihally, S. V. (2005). In vitro characterization of chitosan–gelatin scaffolds for tissue engineering. *Biomaterials*, *26*, 7616–7627.

Jeong, L., Lee, K. Y., Liu, J. W., & Park, W. H. (2006). Time-resolved structural investigation of regenerated silk fibroin nanofibers treated with solvent vapor. *International Journal of Biological Macromolecules*, *38*, 140–144.

Karageorgiou, V., Meinel, L., Hofmann, S., Malhotra, A., Volloch, V., & Kaplan, D. (2004). Bone morphogenetic protein-2 decorated silk fibroin films induce osteogenic differentiation of human bone marrow stromal cells. *Journal of Biomedical Materials Research A*, *71*, 528–537.

Kumbar, S. G., James, R., Nukavarapu, S. P., & Laurencin, C. T. (2008). Electrospun nanofiber scaffolds: Engineering soft tissues. *Biomedical Materials*, *3*, 034002.

Kundu, J., Chung, Y., Kim, Y. H., Tae, G., & Kundu, S. C. (2010). Silk fibroin nanoparticles for cellular uptake and control release. *International Journal of Pharmaceutics*, *388*, 242–250.

Lahiji, A., Sohrabi, A., Hungerford, D. S., & Frondoza, C. G. (2000). Chitosan supports the expression of extracellular matrix proteins in human osteoblasts and chondrocytes. *Journal of Biomedical Materials Research*, *51*, 586–595.

Langer, R., & Vacanti, J. P. (1993). Tissue engineering. *Science*, *260*, 920–926.

Lee, C. H., Shin, H. J., Cho, I. H., Kang, Y. M., Kim, I. A., Park, K. D., & Shin, J. W. (2005). Nanofiber alignment and direction of mechanical strain affect the ECM production of human ACL fibroblast. *Biomaterials*, *26*, 1261–1270.

Lee, H., & Kim, G. (2011). Cryogenically fabricated three-dimensional chitosan scaffolds with pore size-controlled structures for biomedical applications. *Carbohydrate Polymers*, *85*, 817–823.

Li, C., Vepari, C., Jin, H. J., Kim, H. J., & Kaplan, D. L. (2006). Electrospun silk-BMP-2 scaffolds for bone tissue engineering. *Biomaterials*, *27*, 3115–3124.

Li, W. J., Laurencin, C. T., Caterson, E. J., Tuan, R. S., & Ko, F. K. (2002). Electrospun nanofibrous structure: A novel scaffold for tissue engineering. *Journal of Biomedical Materials Research*, *60*, 613–621.

Li, Z. S., Ramay, H. R., Hauch, K. D., Xiao, D. M., & Zhang, M. Q. (2005). Chitosan–alginate hybrid scaffolds for bone tissue engineering. *Biomaterials*, *26*, 3919–3928.

Lieder, R., Reynisdóttir, S. T., Thormódsson, F., Ng, C.-H., Einarsson, J. M., Gíslason, J., Bjórnsson, J., Gudmundsson, S., Petersen, P. H., & Sigurjónsson, O. E. (2012). Glucosamine increases the expression of YKL-40 and osteogenic marker genes in hMSC during osteogenic differentiation. *Natural Products and Bioprospecting*, *2*, 87–91.

Madihally, S. V., & Matthew, H. W. T. (1999). Porous chitosan scaffolds for tissue engineering. *Biomaterials*, *20*, 1133–1142.

Malaval, L., Liu, F., Roche, P., & Aubin, J. E. (1999). Kinetics of osteoprogenitor proliferation and osteoblast differentiation in vitro. *Journal of Cellular Biochemistry*, *74*, 616–627.

Matsuda, A., Kagata, G., Kino, R., & Tanaka, J. (2007). Preparation of chitosan nanofiber tube by electrospinning. *Journal of Nanoscience and Nanotechnology*, *7*, 852–855.

Ogata, K., Imazato, S., Ehara, A., Ebisu, S., Kinomoto, Y., Nakano, T., & Umakoshi, Y. (2005). Comparison of osteoblast responses to hydroxyapatite and hydroxyapatite/soluble calcium phosphate composites. *Journal of Biomedical Materials Research A*, *72*, 127–135.

Ohkawa, K., Cha, D., Kim, H., Nishida, A., & Yamamoto, H. (2004). Electrospinning of chitosan. *Macromolecular Rapid Communications*, *25*(18), 1600–1605.

Omenetto, F. G., & Kaplan, D. L. (2010). New opportunities for an ancient material. *Science*, *329*, 528–531.

Porter, J. R., Ruckh, T. T., & Popat, K. C. (2009). Bone tissue engineering: A review in bone biomimetics and drug delivery strategies. *Biotechnology Progress*, *25*, 1539–1560.

Rim, N. G., Shin, C. S., & Shin, H. (2013). Current approaches to electrospun nanofibers for tissue engineering. *Biomedical Materials*, *8*, 014102.

Setzer, B., Bächle, M., Metzger, M. C., & Kohal, R. J. (2009). The gene-expression and phenotypic response of hFOB 1.19 osteoblasts to surface-modified titanium and zirconia. *Biomaterials*, *30*, 979–990.

She, Z., Jin, C., Huang, Z., Zhang, B., Feng, Q., & Xu, Y. (2008). Silk fibroin/chitosan scaffold: Preparation, characterization, and culture with HepG2 cell. *Journal of Materials Science: Materials in Medicine*, *19*, 3545–3553.

Toskas, G., Cherif, C., Hund, R.-D., Laourine, E., Mahltig, B., Fahmi, A., Heinemann, C., & Hanke, T. (2013). Chitosan(PEO)/silica hybrid nanofibers as a potential biomaterial for bone regeneration. *Carbohydrate Polymers*, *94*, 713–722.

Unger, R. E., Sartoris, A., Peters, K., Motta, A., Migliaresi, C., Kunkel, M., Bulnheim, U., Rychly, J., & Kirkpatrick, C. J. (2007). Tissue-like self-assembly in cocultures of endothelial cells and osteoblasts and the formation of microcapillary-like structures on three-dimensional porous biomaterials. *Biomaterials*, *28*, 3965–3976.

Vepari, C., & Kaplan, D. L. (2007). Silk as a biomaterial. *Progress in Polymer Science*, *32*, 991–1007.

Yamane, S., Iwasaki, N., Majima, T., Funakoshi, T., Masuko, T., Harada, K., Minami, A., Monde, K., & Nishimura, S. (2005). Feasibility of chitosan-based hyaluronic acid hybrid biomaterial for a novel scaffold in cartilage tissue engineering. *Biomaterials*, *26*, 611–619.

Zhang, X., Tsukada, M., Morikawa, H., Aojima, K., Zhang, G., & Miura, M. (2011). Production of silk sericin/silk fibroin blend nanofibers. *Nanoscale Research Letters*, *6*, 510.

Zhang, Y., Lim, C. T., Ramakrishna, S., & Huang, Z. M. (2005). Recent development of polymer nanofibers for biomedical and biotechnological applications. *Journal of Materials Science: Materials in Medicine*, *16*, 933–946.

Zhang, Y., Reddy, V. J., Wong, S. Y., Li, X., Su, B., Ramakrishna, S., & Lim, C. T. (2010). Enhanced biomineralization in osteoblasts on a novel electrospun biocomposite nanofibrous substrate of hydroxyapatite/collagen/chitosan. *Tissue Engineering, A*, *16*, 1949–1960.